Nuclear-to-Outer Rotation Curves of Galaxies in the CO and HI lines

Yoshiaki SOFUE

Institute of Astronomy, University of Tokyo, Mitaka, Tokyo 181, Japan

E-mail: sofue@mtk.ioa.s.u-tokyo.ac.jp

(PASJ, Vol 49, No.1, 1997, in press)

Abstract

We have derived rotation curves of nearby galaxies, which are almost completely sampled from the inner to outer regions. We used high-resolution position-velocity diagrams in the CO line along the major axes for the inner regions, and HI-line data for the outer regions. We combined the CO and HI data to obtain total rotation curves from the nuclear to outer regions. The rotation curves show a steep nuclear rise within a radius smaller than the resolutions of CO-line observations, indicating a compact massive concentration near the nucleus. We show that the nuclear steep rise is general and universal, and a rigid body-like gentle rise is exceptional.

Keywords: Galaxies: kinematics – Galaxies: rotation – Galaxies: structure – Galaxies: general – ISM: CO emission – ISM: HI gas

1. Introduction

Rotation curves (RC) of galaxies obtained by optical (H α) and HI 21-cm line observations have been known to show a rigid-body like increase in the central few kpc region, followed by a flat rotation in the disk and outer regions (Rubin et al 1980, 1982; Bosma 1981b; Persic et al 1995). Since the HI gas is distributed widely in the galactic disk, even extending to the edges of galaxies, HI rotation curves are most useful for investigating the mass distribution in the outer region, and have been used for studying the massive dark halo (Kent 1987). On the other hand, the HI gas is deficient in the central region, where the molecular hydrogen dominates (Sofue et al 1993). CO-line observations have been obtained for a large number of galaxies in the decade (Young and Scoville 1992), and position-velocity diagrams in the central region of these galaxies have been obtained. The CO rotation curves for the nuclear regions have suggested a much sharper rise in the central few hundred parsecs than has been known by HI or optical observations, which has been observed indeed for the Milky Way Galaxy (Clemens 1985).

Combining the CO-line rotation curves for the central regions with HI and optical RC in the outer disks, we have obtained 'most completely sampled rotation curves' for several nearby galaxies (Sofue 1996; Paper I). The radio (CO + HI) rotation curves are found to have a sharp nuclear rise, often associated with a high-velocity peak, in the central few hundred parsecs, then a gap followed by a second maximum at 5 to 10 kpc, and a flatter or slowly declining outer part.

In this paper, we present radio (CO + HI), and optical rotation curves for a larger number of spiral galaxies using high-resolution CO and HI-line data. We aim at clarifying if the nuclear rise of rotation curves is indeed a universal and general characteristic of rotation of spiral galaxies.

2. Envelope-Tracing Method for Deriving Rotation Curves

We adopt the envelope-tracing method as used in Paper I to derive rotation curves, which uses the loci of terminal velocity in position-velocity (PV) diagrams. We define the terminal velocity by a velocity at which the intensity becomes equal to

$$I_{\rm t} = [(0.2I_{\rm max})^2 + I_{\rm lc}^2]^{1/2} \tag{1}$$

on the PV diagrams, where $I_{\rm max}$ and $I_{\rm lc}$ are the maximum intensity and intensity corresponding to the lowest contour level, respectively. This equation defines a 20% level of the intensity profile at a fixed position, $I_{\rm t} \simeq 0.2 \times I_{\rm max}$, if the signal-to-noise ratio is sufficiently high. If the intensity is not high enough, the equation gives $I_{\rm t} \simeq I_{\rm lc}$, which approximately defines the loci along the lowest contour level ($\sim 3 \times$ rms noise). The terminal velocity is then corrected for the velocity dispersion of the interstellar gas ($\sigma_{\rm ISM}$) and the velocity resolution of observations ($\sigma_{\rm obs}$) as

$$V_{\rm t}^0 = V_{\rm t} - (\sigma_{\rm obs}^2 + \sigma_{\rm ISM}^2)^{1/2}.$$
 (2)

Small-scale structures due to clumpy ISM and clouds, and partly due to the noise in the observations, are smoothed by eye estimates. Since it was not practical to apply these procedures automatically by a computer, we have drawn the curves by hand on each position-velocity diagram. The rotation velocity is finally obtained by

$$V_{\rm rot} = V_{\rm t}^0 / \sin i, \tag{3}$$

where i is the inclination angle of the disk plane. The accuracy of determining the terminal velocity, and therefore, the accuracy of the obtained rotation curve was typically $\pm 10 \sim 15/\sin i \text{ km s}^{-1}$.

Simply-traced envelopes on the two sides of the nucleus have a discontinuity at the nucleus due to the finite beam width. We have avoided this discontinuity by stopping the tracing at a radius corresponding to the telescope resolution, and then by connecting the both sides of rotation curve by a straight (solid-body like) line crossing the nucleus at zero velocity. Figure 1 shows examples of the CO-line position-velocity diagrams and traced rotation curves for several galaxies, combined with HI rotation curves. The pair of rotation curves thus obtained on both (receding and approaching) sides of the nucleus are finally averaged to give a rotation curve as a function of the radius. The inner rotation curves thus derived from CO-line data were, then, connected smoothly to the HI curves in the outer disk. In most cases the discrepancy between CO and HI rotation velocities at the connecting area were within about ± 10 kms. Since the CO data usually have higher resolution than HI, we adopted CO curves, when both CO and HI curves were available at the same radius.

3. CO + HI Rotation Curves for Individual Galaxies

Figure 2 shows the obtained radio (CO+HI) rotation curves for the studied galaxies with the basic data inserted, such as the inclination, position angle of the major axis, and a possible distance taken from the literature cited in table 1. These distances are often uncertain, and therefore, the linear scales indicated along the upper ordinates are also uncertain. Vertical bars of the crosses represent the typical errors in velocity determination, and the horizontal bars indicate the angular resolutions of observations. Vertical dashed lines separate each rotation curve into two or three parts, where the CO and HI data have been used, respectively. When different data with different angular resolutions are combined, their border is also indicated by a dashed line. We show by inset optical images of the galaxies taken from the STScI Digitized Sky Survey (DSS). A $10' \times 10'$ field is displayed for each object (larger fields for a few galaxies), and the angular scale is given along the major axis. We describe the individual galaxies below. Parameters and references for the data are listed in Table 1.

NGC 224 (M31): This galaxy is one of the few exceptional nearby galaxies of Sb type, which emit very weak CO line in the center: Even in our deep observation with the Nobeyama 45-m telescope we could detect only weak or almost no CO emission in the nuclear region (Sofue and Yoshida 1993). Therefore, no sufficient kinematical data are available to derive a CO rotation curve. However, there have been a number of studies of the rotation curve as summarized in Sofue and Kato (1981). We revisited and obtained a new RC using the optical data in the [NII] λ 6583 emission observed by Rubin and Ford (1970) and in the H α line by Ciardullo et al. (1988). We adopted the H α velocities for the very inner region within 1', and those from [NII] line for the inner 6', where the rotation rises steeply to a peak velocity of 220 km s⁻¹ at 2' radius. Beyond this radius, we adopted the HI data from the Bonn 100-m telescope, which is sensitive enough to trace the rotation with a sufficient accuracy, although the resolution (9') was not enough to resolve the

innermost region. The HI position-velocity diagram shows a pair of symmetrical shoulders at $\pm 10'$ with respect to the nucleus, corresponding to the central peak indicated by the optical observations. The velocity, then, increases to a maximum as high as 280 km s⁻¹ at 40', and declines slowly toward the edge.

NGC 253: This is a CO-rich starburst galaxy, and has been studied in Paper I based on a lower-resolution CO data. We revisited this galaxy using the higher-resolution CO data from the 45-m telescope. The central peak of rotation curve is more clearly seen in the new data. See Paper I.

IC 342: A central rise and a step, corresponding to the nuclear peak at 130 km s⁻¹, is followed by an almost flat rotation in the disk and outer part. See Paper I.

NGC 598 (M33): Because of its proximity, we used lower-resolution CO data from the Kitt Peak 12-m telescope, which we combine with the HI rotation curve. The CO rotation observed for the inner 5' region agrees with the HI rotation. The rotation velocity increases steeply near the nucleus, but reaches only to 20 km s⁻¹, and turns to increase more gently from the inner 1' region to 10'. It continues to increase monotonically to the observed edge at 30'. This galaxy shows neither a steep rise nor a sharp central peak, similarly to NGC 4631, and is exceptional among the galaxies studied here. Note that both M33 and NGC 4631 are low-mass galaxies.

NGC 660: This is a nearly edge-on Sc galaxy with a polar ring (van Driel et al. 1995). We applied the envelope-tracing method to the HI position-velocity diagrams for the disk and polar ring, as well as to the CO (2-1) position velocity diagram for the inner part. The disk rotation curve can be apparently connected smoothly to that of the polar ring. Since the polar-ring rotation will manifest the gravitational potential in the halo, which is supposed to be round, we may approximate the outer rotation curve in the disk plane by this polar ring curve. The CO line profiles indicate that the maximum rotation velocity occurs near the center, in an unresolved region of < 10''. The inner CO rotation has a high central peak of about 190 km s⁻¹, followed by a disk rotation, where HI and CO velocities coincide well.

NGC 1068: This is a Seyfert galaxy. The position angle of the major axis is not well defined. We adopted 70° for the outer and disk region as read from the outer optical velocity field as well as from the optical image, and 90° for the central region from the CO velocity field (see the literature cited in Table 1). The rotation velocity apppears to rise steeply in the center toward the peak on the molecular ring. However, the very central behavior is not observed due to the lack in the CO emission at the center.

NGC 1097: If the adopted inclination angle of 40° is correct, the apparent rotation velocity of the molecular ring is as high as 350 km s^{-1} , showing a nuclear peak. The rotation decreases then to a dip at 40'' radius, followed by a broad maximum of about 300 km s^{-1} at 2', and then flattens and slowly declines toward the edge. The general characteristic is similar to that of the Milky Way, except the velocity amplitude.

NGC 1365: This is a typical barred spiral with a Seyfert nucleus. The CO data from the SEST 15-m telescope indicate a steep rise and a central peak at 240 km $\rm s^{-1}$, followed by a disk component as high as 270 km $\rm s^{-1}$, and then a monotonically declining rotation observed in the HI line.

NGC 1808: A steep nuclear rise and a peak are followed by a gradual decrease toward the edge of the observed rotation curve. See Paper I.

NGC 2403: Due to its proximity, we used the lower-resolution CO data from the Kitt Peak 12-m telescope. No higher-resolution observations are available. The RC increases steeply in the center till 80 km s⁻¹, then increases slowly till 5' radius, where the curve turns to be flat at a velocity as low as 120 km s⁻¹. The CO and HI curves agree with each other at 1' to 5', while CO velocity is much higher in the central 1' region.

NGC 2841: Since no high-resolution CO data are available, we used the FCRAO 14m CO data for the inner 4' to derive a CO rotation curve, and combined it with the outer HI rotation curve. Although the very central kinematics is not clear due to the weak CO emission near the nucleus, a steep rise within the central 1' region and a peak as high as 310 km s⁻¹ are visible. After increasing to a maximum of 330 km s⁻¹ at 2 to 3', the velocity decreases and turns to be flat at 270 km s⁻¹until the edge.

NGC 2903: The CO rotation curve has a peculiar step at 1-2' radius with a maximum of about 170 km s⁻¹ at 1'. It, then, increases to a second maximum of 200 km s⁻¹ at 3'. The step is, however, asymmetric with respect to the center: This inner maximum has a higher velocity in the SW side than in the NE. The outer rotation from HI is, however, very flat until the edge.

NGC 3031 (M81): Optical and CO-line data have been combined for the central 2'. The rotation has a central peak at 300 km s⁻¹, although the peak is not very sharp. The HI rotation from the disk to outer

region is similar to that of the Milky Way in shape and velocity.

NGC 3034 (M82): This is an interacting peculiar galaxy with a starburst activity and is rich in CO gas. The CO (J = 2-1) data obtained by the IRAM 30-m telescope show a clearly declining rotation curve, well fitted by a Keplerian rotation. The VLA HI data agree with the CO data, though the error is larger.

NGC 3079: Sharp and high-velocity nuclear rise and a peak, and then a gap, are followed by a disk component, similar to that of the Milky Way. The outer rotation is declining. See Paper I.

NGC 3198: The central steep rise stops at a peak as low as 50 km s^{-1} . Then, the rotation increases in a rigid-body fashion, showing a next step. The disk part has a broad maximum of 170 km s^{-1} , followed by a flat rotation.

NGC 3521: The inner rotation curve increases steeply, and attains a small and sharp central peak at 10'' of 210 km s⁻¹, followed by a dip at 20''. Then, it increases slowly till a broad maximum at 1'.5. The outer HI RC gradually decreases till the edge.

NGC 3628: The CO PV diagram as obtained by interferometer observations with the Nobeyama Millimeter Array shows a nuclear disk asymmetric with respect to the position-velocity center of the outer disk. We took the center of the nuclear disk as the origin of the rotation curve, and connected the inner RC with the outer rotation curve by averaging the position and velocities in both sides of the nucleus. The CO+HI RC has a steep rise near the center within 5'', indicating a nuclear disk, rotating at 190 km s⁻¹. It further increases to 200 km s⁻¹ at 1', and is followed by a flat rotation in the outer disk.

NGC 4258: The velocity increases to a maximum of 230 km s⁻¹within the central 30", and decreases to a flat part at 3 to 7'. The outer HI rotation is almost flat, after a broad maximum at 10' radius.

NGC 4303: The rotation curve for the central 15" has been derived using a position-velocity diagram at a constant declination obtained by the NMA. The correction for position-angle and inclination resulted in a high velocity peak, which is not clearly seen in the 45-m data. The error for the central peak is, therefore, as large as $\sim 30 \text{ km s}^{-1}$. The disk and outer parts of the rotation curve are flat.

NGC 4321 (M100): The NMA observation shows a steeply increasing rotation within a 5'' radius to a central peak of 230 km s⁻¹ at 10'', followed by a dip at 20''. The RC, then, increases gradually till 3' to a broad maximum of 270 km s^{-1} in HI velocity. The outermost rotation velocity is not certain because of the warped HI disk and low inclination.

NGC 4565: This is a typical edge-on galaxy of Sc type. The rotation has a central peak and a flat disk-to-outer rotation. It has a sign of declining in the outermost region. See Paper I.

NGC 4569: This is Virgo galaxy which shows a truncated HI gas disk. CO-line position-velocity diagrams obtained with the NMA at a 9" resolution show a sharp rise to a 200 km s⁻¹ central peak. The 45-m data show a rotation minimum at 40", followed by an increase toward the HI high-velocity rotation in the outer disk. The outskirts of HI gas are missing due possibly to a ram-pressure stripping by the intra-cluster gas.

NGC 4631: This is an interacting, edge-on semi-dwarf galaxy. The CO RC in the central 40" is rigid-body like, having neither a nuclear rise nor a peak. The RC is followed by a flat and declining HI rotation in the outer disk. This galaxy is one of the two exceptions (with M33), which show no nuclear rise of rotation in CO. However, the intensity distribution along the major axis indicates no concentration of CO gas in the center, but either a ring or clumps avoiding the nucleus (Sofue et al. 1989). Therefore, the apparent rigid-body rotation in the position-velocity diagram may be due to the lack of gas near the nucleus, even if the true rotation curve has a sharper rise.

NGC 4736: The rotation rises steeply within 12", and attains a central peak at 18". It, then, decreases monotonically toward the observed edge.

NGC 4945: We used position-velocity diagrams along the major axis from the two-elements interferometric observations to derive an HI rotation curve, and those from the SEST 15-m observations in the CO (J=1-0) and CO (J=2-1) emissions. We adopted the higher-resolution CO (2-1) data for the inner region, CO (1-0) for the disk, and HI for the outer region. They agree in the overlapped regions, except that the CO (2-1) data indicated a shaper central peak of RC than CO (1-0). The obtained RC is similar to that of our Galaxy. It has a steep rise and a sharp central peak, followed by a broad maximum in the disk and a flat part in the outskirts.

NGC 5033: A sharp rise to a central peak at 10" is followed by a second peak at 35". The outer HI rotation is flat till the edge, indicating a sign of declining rotation near the edge.

NGC 5055: A sharp, rigid body-like rise within the central 30" is followed by a flat part till a broad

maximum at 4'. The rotation declines then till 8', beyond which it is nearly flat.

NGC 5194 (M51): A steep rise in the center is followed by a flat disk rotation till 2'.7 radius, superposed by high-amplitude velocity deviation due to the spiral arms. The rotation velocity, then, declines more rapidly than a Keplerian curve. This may be due to the gravitational disturbance by the companion NGC 5195, or to a warp in the outer disk likely caused by the tidal interaction. See Paper I.

NGC 5236 (M83): The RC rises very steeply near the center, attaining a sharp peak at 10'' of 250 km s⁻¹. It, then, decreases steeply toward a deep dip at 30'' with a minimum velocity as low as 120 km s^{-1} . The RC again increases toward a second broad maximum at 2' of 190 km s^{-1} , and is followed by a gradually declining HI part in the outer disk. The sharp central peak and deep dip are peculiar among the galaxies so far known of the rotation curves, and may be related to the bar and accretion process.

NGC 5457 (M101): This is a nearly face-on Sc galaxy, but no high-resolution CO data are available. Because of its large apparent size, we used lower-resolution CO data from the Kitt Peak 12-m telescope. The central rise within the beam width 30'' is recognized, but the resolution is not sufficient for discussing the detail about the nuclear rise.

NGC 5907: This is an almost perfectly edge-on galaxy. The central RC rises steeply to a shoulder of 200 km s^{-1} at 10''. The RC further continues to increase till 4' radius, and, then, declines toward the edge. See Paper I.

NGC 6946: The central peak is very sharp and as high as 240 km s^{-1} , followed by a gap which is rather flat till the second increase toward the disk maximum starts. This rotation curve is similar to that of the Milky Way. See Paper I.

NGC 6951: The central high-velocity peak of 260 km s⁻¹ is remarkable at a radius of 20". Since the resolution of the 45-m telescope is not enough to resolve this region due to the relatively large distance, the true peak velocity may be much higher. The CO RC has been combined with the H α data for the disk part, showing a gradually increasing toward the outer region.

NGC 7331: The central steep rise has a shoulder-like step of 130 km s⁻¹ at 14", and reaches a peak of 240 km s⁻¹ at 34" after a rigid-body like increase. The outer HI rotation is almost flat, slightly increasing till the end of the disk.

Milky Way: For a comparison, we show the rotation curve for our Galaxy. The Sun's distance from the nucleus is taken to be 8 kpc. The RC within the solar circle was taken from Clemens (1995), and that for the outer region from Honma and Sofue (1996a, b). See the literature for details.

4. Discussion

4.1. Steep Nuclear Rise

We have derived the CO rotation curves of the central regions for nearby spiral galaxies, and combined them with outer HI rotation curves. A remarkable feature obtained in the present study is the steep nuclear rise of rotation within a radius smaller than the beam width of CO observations. Two exceptional cases were found: A nearby Sc galaxy M33 known for the low surface brightness shows a rapid rise in the center, but to a low velocity, and then a gentle rise; NGC 4631, a semi-dwarf edge-on galaxy of amorphous type, has a rigid-body rise. However, NGC 4631's case might be an apparent phenomenon due to the lack of CO gas near the center, and the true rotation curve may have a sharper rise. Hence, the only one exception having indeed a slowly rising rotation is M33.

4.2. The Nuclear Mass Component

In Paper I we have shown that the steeply rising rotation curves can be generally fitted by a model with four mass components: the nuclear compact mass, central bulge, disk, and the massive halo. Particularly, such a steep rise within the central few hundred parsecs as observed for NGC 3079, NGC 4321 and NGC 6946

by high-resolution interferometer observations indicates the existence of a compact nuclear mass of a 100 to 150 pc radius and a mass of several $10^9 M_{\odot}$. Hence, some of the galaxies are likely to be nested by a more compact stellar mass concentration in the center than the usual bulges, which we called a bulge-in-bulge.

In order to avoid the discontinuity of envelope-traced terminal velocities from both sides of the nucleus on the position-velocity diagrams, we have connected them by a solid-body like line crossing the nucleus at zero velocity within a radius comparable to the angular resolution. Therefore, the curves drawn within the regions smaller than the angular resolution may not represent the true velocities. It is more likely that the true rotation curve has a sharper, unresolved rise. It is also likely that the velocity remains finite till the nucleus, or even increases, since the galactic nuclei are often nested by a compact massive object.

4.3. Circular Rotation-vs-Bar Debate

By definition, a rotation curve is the trace of terminal velocities in the position-velocity diagram along the major axis. It may be superposed by non-circular motions such as due to the density waves, bars and oval potential, or interaction with the companion. It is, therefore, not straightforward to derive the mass distribution using the curves by assuming a circular rotation. Nevertheless, this assumption has been extensively adopted in deriving the mass of galaxies including hypothetical dark halos. The mass and potential derived from the circular-rotation assumption has also been used to discuss the inner and outer Lindblad resonances or to analyze the pattern speed and density waves. Rotation curves have also been used to derive the mass distributions in the bulges and central cores, and have given a good agreement with the surface photometry (e.g., Kent 1987). These studies have made available the most important parameters of the galaxies, and the circular-rotation assumption appears reasonable in so far as the basic structures of galaxies are analyzed.

On the other hand, it is a trend to introduce a bar in the analysis. However, if one stands on a bar hypothesis, the so-called rotation curves will give no more any quantitative information about the mass, unless the true potential is determined by independent observations. One might argue that the nuclear rise and peak of rotation may be due to a high-velocity flow of gas along a bar parallel to the line of sight, whereas the mass (potential) distribution is not known, which is necessary to calculate the flow. However, the probability of looking at a bar from its end is far smaller compared to that of looking at it at a finite angle. In the latter case, the gas along the bar will be observed roughly at the bar's pattern speed, and, therefore, will show a rigid-body like rotation at lower velocities than a circular rotation. Hence, if some cases of the nuclear rise of rotation are due to a bar indeed, a larger number of galaxies must be observed to show a gentle rise in a rigid-body fashion. This is, however, not the case at all. Note that M33 has no bar, and NGC 4631 is an amorphous dwarf and does not provide a firm case for rigid body rotation. Hence, it is not likely that the nuclear rise observed in almost all galaxies studied here is due to a bar-induced gas flow.

We may, therefore, reasonably assume that the central rotation is circular in the zero-th order approximation, and the observed rotation curves manifest the mass distribution within the bulges. This can be clarified by comparing the observed rotation curves with those calculated by a mass model based on a surface photometry assuming an appropriate mass-to-light ratio, as has been obtained for disk regions by Kent (1987) on the basis of optical data. Since the nuclear region is highly obscured in optical wavelengths, we may need infrared surface photometry for the comparison, which will be described in a separate paper.

References

Ables, J. G., et al. 1987 MNRAS 226, 157

Begeman, K. G. 1989 A&A 223, 47

Bosma, A., van der Hulst, M., Sullivan, III., W. T. 1977

Bosma, A., Goss, W. M., Allen, R. J. 1981 A&S 93, 106.

Bosma, A. 1981a, AJ 86, 1791.

Bosma, A. 1981b, AJ, 86, 1825.

Bosma, A., van der Hulst, J. M., Sulivan, III, W.T. 1977, A&A 57, 373.

Clemens, D. P. 1985 ApJ 295, 422.

Casertano, S. 1983, MNRAS, 203, 735.

Casertano, S., van Gorkom, J. H. 1991, AJ 101, 1231.

Ciardullo, R., Rubin, V.C., Jacoby, G. H., Ford, H. C., and Ford, Jr. W. K. 1988 AJ 95, 438.

Combes F 1992 ARA&A, 29, 195.

Combes, F., Gottesman, S. T., Weliachew, L. 1977 A&A 59, 181

Cram, T. R., Roberts, M. S., and Whitehurst, R. N. 1980 A&AS 40, 215.

Dahlem, M., Golla, G., Whiteoak, J. B., Wielebinski, R., Hüttemessiter, S., and Henkel, C. 1993 A&A 270, 29

Gerin, M., Nakai, N., Combes, F. 1988, A&A 203, 44

Goad, J. W. 1976 ApJS 32, 89

Guhathakurta, P., and van Gorkom, J. H. 1988 AJ 95, 851.

Honma, M., and Sofue, Y. 1996a PASJ, submitted

Honma, M., and Sofue, Y. 1996b PASJ Letter, in press.

Hunter, D. A., Rubin, V.C., R. and Gallagher, J. S., III 1986 AJ 91, 1086

Irwin, J.A. and Sofue, Y. 1996, ApJ 464, 738

Kaneko, N., Satoh, T., Toyama, K., Sasaki, M., Nishimurfa, M., Yamamoto, M. 1992 AJ 103, 422

Kaneko, N., Morita, K., Fukui, Y., Takahashi, N., Sugitani, K., Nakai, N. Morita, K. 1992 PASJ 44, 341.

Kaneko, N., Morita, K., Fukui, Y., Sugitani, K., Iwata, T., Nakai, N. Kaifu, N., Liszt, H. 1989 ApJ 337, 691.

Kenney, J., Young, S. J. 1988 ApJS 66, 261.

Kenney, J. D. P., Scoville, N. Z., and Wilson, C. D. 1991 ApJ 366, 432.

Kent, S. M. 1986 AJ 91, 1301.

Kent, S. M. 1987 AJ 93, 816.

Knapen, J. H., Cepa, J., Beckman, J.E., Soledar del Rio, M., Pedlar, A. 1993 ApJ 416, 563

Knapen, J. H., Beckman, J. E., Heller, C. H., Shlosman, I. De Jong R. S. 1995 ApJ, 454, 623

Newton, K. 1980 MNRAS 190, 689

Lake, G. and Feinswog, L. 1989 AJ 98 166

Marguez, I., Moles, M. 1993, AJ 105, 2050.

Nishiyama, K. 1995 PhD Thesis, University of Tokyo

Ondrechen, M. P., van der Hulst, J. M. 1989 ApJ 32, 29.

Ondrechen, M. P., van der Hulst, J. M., Hummel, E. 1989 ApJ 342, 39O

Planesas, P., Scoville, N., Myers, S. T. 1991 ApJ 369, 364.

Persic, S., Salucci, P., Stel, F. 1996 MNRAS.281, 27.

Rots, A. H. 1975 A&A 45, 43

Rubin, V. C., and Ford, Jr. W. K. 1970 ApJ 159, 381

Rubin, V. C., Ford, W. K., Thonnard, N. 1980, ApJ, 238, 471

Rubin, V. C., Ford, W. K., Thonnard, N. 1982, ApJ, 261, 439

Sage, L. I., and Westpfahl, D. J. 1991 A&A 242, 371

Sakamoto, K. 1995 PhD Thesis, University of Tokyo

Sakamoto, K., Okumura, S., Minezaki, T., Kobayashi, Y., Wada, K. 1995 AJ 110, 2075

Sandqvist, Aa., Jörsäster, S., and Lindblad, P.O. 1995 A&A 295, 585.

Sofue, Y. 1996, ApJ, 458, 120 (Paper I)

Sofue, Y., Doi, M., Krause, M., Nakai, N., and Handa, T. 1989 PASJ 41, 113

Sofue, Y., Handa, T., and Nakai, N. 1989 PASJ 41, 937.

Sofue, Y., Handa, T., G. Golla, M. Krause, and R. Wielebinski 1990, PASJ 42, 745

Sofue, Y., Honma, M., Arimoto, N. 1994, A&A 296, 33-44.

Sofue, Y. and Kato, R. 1981 PASJ

Sofue, Y., Reuter, H.-P., Krause, M., Wielebinski, R., and Nakai, N. 1992 ApJL 395, 126.

Sofue, Y., Tutui, Y., Honma, M. 1997 in preparation

Sofue, Y., and Yoshida, Y. 1993, ApJL 417, L63

Thornley, M. D., and Wilson, C. D. 1995 ApJ 447, 616.

van Albada, G.D. and Shane, W.W. 1976 A&A 42, 433.

van Driel, W. et al 1995 AJ 109, 942

Weliachev, L., Sancisi, R., Guélin, M. 1978 A&A 65, 37.

Wilding, T., Alexander, P., and Green, D. A. 1993 MN 263, 1075

Wilson, C. D., Scoville, N. 1989 ApJ 347, 743.
Young, J. S., Scoville, N. Z. 1992, ARA&A, 29, 581.
Young, J.S., et al. 1995 ApJS 98, 219
Yun, M. S., Ho, P.T.P, and Lo, K.Y. 1993 ApJL 411, L17.

Figure Captions

Fig. 1: Examples of position-velocity diagrams in the CO line emission for some galaxies, and traced rotation curves, which are smoothly connected with HI rotation curves. Crosses indicate typical errors (vertical) and angular resolution (horizontal).

Fig. 2: Inner-to-out rotation curves obtained by combining CO and HI rotation curves of galaxies. Some curves have been obtained by using optical data. Typical angular resolutions and errors are indicated by crosses at several representative points for each object. The horizontal bars indicate the angular resolutions, and the vertical bars give errors in the rotation velocity estimates. Dashed vertical lines indicate the borders of CO and HI rotation curves. Borders of regions with different data of different angular resolutions are also marked by dashed lines. Optical images from the STScI Digital Sky Survey are shown with the major axes and angular scales superposed.

Table 1: Parameters for galaxies and references for PV diagrams and rotation curves.

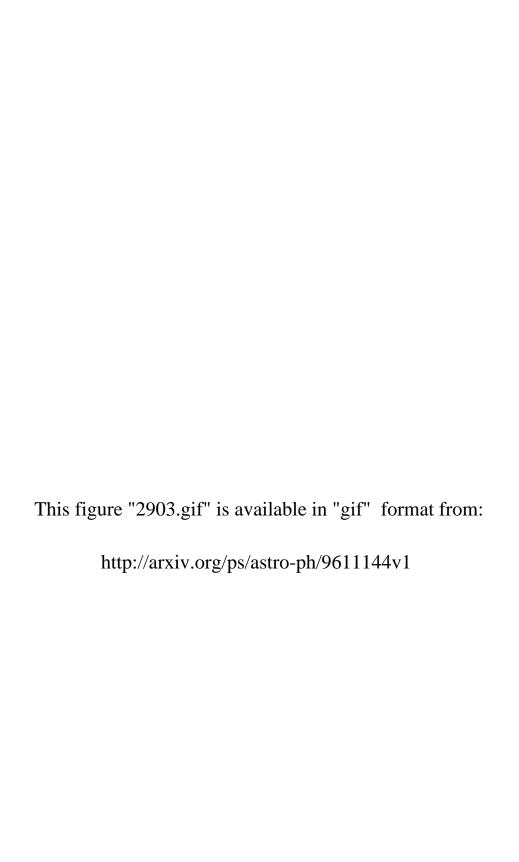
Galaxy Type	$\begin{array}{c} {\rm Incl.} \\ {\rm (deg)} \end{array}$	$^{\mathrm{Dist.*}}_{\mathrm{(Mpc)}}$	Line	$\mathrm{Telescope}^{\dagger}$	A. Reso. (a.sec)	References
NGC 224 (M31) Sb 7	7	0.69	$\begin{array}{c} \text{Opt.[NII]} \\ \text{H}\alpha \\ \text{HI} \end{array}$	E100m	540	Rubin & Ford 1970 Ciardullo et al. 1988 Cram et al. 1980
NGC 253 Sc	78.5	2.5	CO	 N45m	 15	Paper I Nishiyama 1995
IC 342 Sc	25	3.9				Paper I
NGC 593 (M33) Sc 5	4	0.79	HI CO	CI K12m	47 55	Newton 1980 Wilson & Scoville 1989
NGC 660 Sc Polar ring	70	13	HI HI CO 2-1	W W I30m	20 60 12	van Driel et al. 1995 ibid ibid
NGC 891 Sb	88.3	8.9				Paper I
NGC 1068 Sb Sy	46	18.1	Opt. Opt CO CO	N45m NMA	$\begin{array}{c} 17 \\ 5 \times 4 \end{array}$	Kaneko et al. 1992 Galleta &Recillas-Cruz 1982 Kaneko et al 1991 Kaneko et al 1992
NGC 1097 SBb	40	16	CO HI	$_{ m V}^{ m N45m}$	15 25	Gerin et al. 1988 Ondrechen et al. 1989
NGC 1365 SBb	46	15.6	HI CO 2-1	m V m S15m	$\begin{array}{c} 36 \times 23 \\ 25 \end{array}$	Ondrechen & van der Hulst 1989 Sandqvist et al. 1995
NGC 1808 Sbc	58	11.4				Paper I
${\rm NGC~2403~Sc}$	60	3.25	HI CO	m W m K12m	40/60 60	Lake & Feinswog 1989 Thornley & Wilson 1995
NGC 2841 Sb	68	9	HI CO	m W m F14m	$51 \times 65 \text{ B}$ 45	osma 1981a Young et al. 1995
${\rm NGC~2903~Sc}$	35	6.1	HI CO	m W m N45m	15	Lake & Feinswog 1989; Kent 1987 Sofue et al 1997
NGC 3031 (M81) Sb	59	3.25	Opt CO HI	K12m W	55 25/50	Goad 1976 Sage & Westpfahl 1991 Rots 1975
NGC 3034 (M82) Ir 8	80-90	3.25	CO 2-1 HI	$_{ m V}^{ m I30m}$	13 18	Sofue et al 1992 Yun et al. 1993
NGC 3079 Sc	~ 90	15.6	• • • • • • • • •			Paper I

NGC 3198 SBc	70	9.1	HI HI Opt	W W	25×35 25×35	Bosma 1981a Begeman 1989 Hunter, et al. 1986	
NGC 3521 Sbc	75	8.9	HI CO	m W m N45m	74×53 15	Casertano, van Gorkom 1991 Sofue et al 1997	
NGC 3628 Sb(Ir) > 86	ŝ	6.7	CO HI	NMA V	3.9 15	Irwin & Sofue 1995 Wilding et al 1993	
NGC 4258 Sbc	67	6.6	HI CO	m W N45m	40 15	van Albada & Shane 1976 Sofue et al 1989	
NGC 4303 Sc	27	8.1	CO CO HI	N45m NMA V	15 4 45	Nishiyama 1995 Sofue et al. 1997 Guhathakurta et al 1988	
NGC 4321 (M100) Sc	27	15	CO CO HI	N45m NMA V	15 4	Nishiyama 1995 Sakamosto 1995 Knapen et al 1993	
NGC 4565 Sb	86	10.2				. Paper I	
NGC 4569 Sab	63	8.2	CO CO HI	N45m NMA V	$15 \\ 9.9 \times 4.8 \\ 20$	Nishiyama 1995 Sofue et al 1997 Guhathakurta & van Gorkom	
${\rm NGC~4631~Sc~Ir}$	84	5.2	HI CO CO(2-1)	W N45m I30m	48×89 15 13	Weliachev et al 1978 Sofue et al. 1989, 1997 Sofue et al. 1990	
NGC 4736 Sab	35	5.1	CO HI	$_{ m W}^{ m N45m}$	15 25×38	Nishiyama 1995 Bosma et al 1977	
${\rm NGC~4945~Sc~I}$	78	6.7	CO(2-1) CO(1-0) HI	$\begin{array}{c} { m S15m} \\ { m S15m} \\ { m TE} \end{array}$	24 43	Dahlem et al 1993 ibid Ables et al. 1987	
${\rm NGC~5033~Sc}$	62	14	CO HI	m N45m $ m W$	$15 \\ 51 \times 85$	Nishiyama 1995 Bosma 1981a	
NGC 5055 Sbc	55	8	HI CO	m W N45m	49×73 15	Bosma 1981a Sofue et al 1997	
NGC 5194 (M51) Sc 20		9.6	Paper I				
NGC 5236 (M83) SBc 24		8.9	CO HI	m N45m $ m W$	15 40	Handa et al 1978, Nishiyama 1995 Bosma et al. 1981	
NGC 5457 (M101) Sc	18	7.2	HI CO	m W m F14m	24×30 50	Bosma et al. 1981 Kenney et al 1991	
NGC 5907 Sc	88	11.6				. Paper I	

NGC 6946 Sc	30	5.5	Paper I				
NGC 6951 Sbc	48		CO Opt	N45m	15	Nishiyama 1995 Marquez, Moles 1993	
NGC 7331 Sbc	75	14	HI CO	m W m N45m	25×45 15	Bosma 1981a Sofue et al 1997	
Milky Way Sb (outside solar circ	90 ele)	0	CO+HI HI			Clemens 1995 Honma & Sofue 1996a,b	

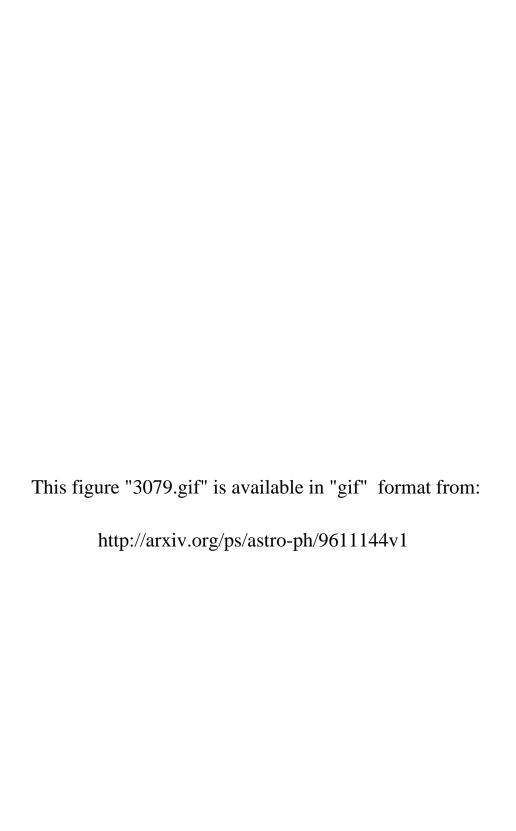
^{*} Distances have been taken from the references in the same row. For the original data, refer to the literature.

^{† (}CO-line observations) N45m = NRO 45-m telescope; I30m = IRAM 30-m telescope; S15m = SEST 15m telescope; F14m = FCRAO 14-m telescope; K12m = NRAO Kitt-Peak 12-m telescope; NMA = Nobeyama Millimeter Array. (HI-line observations) E100m = Effelsberg 100-m telescope; CI = Cambridge Interferometer; W = WSRT; V = VLA; TE = Two-Element Synthesis telescope. (Optical observations) Opt = Optical line (e.g., $H\alpha$) observations.



This figure "3031.gif" is available in "gif" format from:

This figure "3034.gif" is available in "gif" format from:



This figure "3198.gif" is available in "gif" format from:

This figure "3521.gif" is available in "gif" format from:

This figure "3531.gif" is available in "gif" format from:

This figure "3628.gif" is available in "gif" format from:

This figure "4258.gif" is available in "gif" format from:

This figure "4303.gif" is available in "gif" format from:

http://arxiv.org/ps/astro-ph/9611144v1

This figure "4321.gif" is available in "gif" format from:

This figure "4565.gif" is available in "gif" format from:

This figure "4569.gif" is available in "gif" format from:

This figure "4631.gif" is available in "gif" format from:

This figure "4736.gif" is available in "gif" format from:

This figure "4945.gif" is available in "gif" format from:



This figure "7331.gif" is available in "gif" format from: